Toxicon 153 (2018) 106–113

Contents lists available at ScienceDirect

Toxicon

journal homepage: www.elsevier.com/locate/toxicon

Review

Modeling and molecular dynamics indicate that snake venom phospholipase B-like enzymes are Ntn-hydrolases

Mônika Aparecida Coronado[a,*,1], Danilo da Silva Olivier[a,1], Raphael Josef Eberle[a], Marcos Serrou do Amaral[b], Raghuvir Krishnaswamy Arni[a,**]

[a] Multiuser Center for Biomolecular Innovation, Department of Physics, Universidade Estadual Paulista, UNESP/Ibilce, São Jose do Rio Preto, SP, Brazil
[b] Institute of Physics, Universidade Federal de Mato Grosso do Sul, Campo Grande, MS, Brazil

ARTICLE INFO

Keywords:
Snake venom phospholipase B
Crotalus adamanteus
Ntn-hydrolase
Molecular modeling
Molecular dynamics

ABSTRACT

Phospholipase-B-like (SVPLB-like) enzymes are present in relatively small amounts in a number of venoms, however, their biological function and mechanisms of action are un-clear. A three-dimensional model of the SVPLB-like enzyme from *Crotalus adamanteus* was generated by homology modeling based on the crystal structures of bovine Ntn-hydrolyases and the modeled protein possesses conserved domains characteristic of Ntn-hydrolases. Molecular dynamics simulations indicate that activation by autocatalytic cleavage results in the removal of 25 amino acids which increases accessibility to the active site. SVPLB-like enzymes possess a highly reactive cysteine and are hence amidases that to belong to the N-terminal nucleophile (Ntn) hydrolase family. The Ntn-hydrolases (N-terminal nucleophile) form a superfamily of diverse enzymes that are activated autocatalytically; wherein the N-terminal catalytic nucleophile is implicated in the cleavage of the amide bond.

1. Introduction

The functional and structural aspects of snake venom proteins that are relatively abundant have been extensively studied, and their three-dimensional structures, mechanisms of action and specificities are now understood in detail and have been presented in recent reviews (Kang et al., 2011; Coronado et al., 2014, 2016). Advances in proteomics have contributed greatly to the identification of enzymes that are present only in very low concentrations in venoms, such as glutathione peroxidase, 5´ nucleotidase, carboxipeptidase phosphodiesterase, glutaminyl cyclase and phospholipase B (Ohler et al., 2010; Georgieva et al., 2010; Pla et al., 2018; Oliveira et al., 2018). Counterparts of most of these enzymes from other sources have been studied and by extension, most of the conclusions from these studies can be applied to snake venom enzymes (Kang et al., 2011). One exception is snake venom phospholipase B (SVPLB), which, by definition, should participate in the hydrolysis of phospholipids. Multiple sequence alignments indicate that the SVPLBs share high sequence identity with the Ntn-hydrolases, a superfamily of enzymes that display common structural features and catalyzes the hydrolysis of specific amide bonds in substrates ranging from antibiotics to proteins (Brannigan et al., 1995; Suresh et al., 1999).

Ntn-hydrolases are post-translationally activated by an autocatalytic process that cleavages and liberates a peptide of 25 amino acids. The enzymes function via a catalytic mechanism that involves a single amino acid (Thr, Ser or Cys) along with the newly generated N-terminal amino group, which serves both as a nucleophile and as the catalytic base (Duggleby et al., 1995; Suresh et al., 1999; Kim et al., 2000, 2006; Rawlings et al., 2018).

Phospholipase B calcium-independent PLA_2 ($iPLA_2$) (Ackermann and Dennis, 1995; Akiba and Sato, 2004) and PLB activity have been reported in different classes of organisms as in Streptomyces sp (Matsumoto et al., 2013), *Penicillium notatum* (Dawson, 1958; Ghannoum, 2000), *Guinea pig* (Nauze et al., 2002), as well as in plants (Gallard, 1971; Matsuda and Hirayama, 1979) and rabbits (*Oryctolagus cuniculus*) (Boll et al., 1993). Doery and Pearson (1964) observed this activity in the venom of Australian elapid snakes. Since then, several SVPLBs enzymes have been purified and characterized for example from the venoms of *Pseudechis porphyriacus* (Doery and Pearson, 1964), *Pseudechis colletti* (Bernheimer et al., 1987), *Crotalus adamanteus* (Rokyta et al., 2011), *Drysdalia coronoides* (Chatrath et al., 2011), *Ophiophagus hannah* (Vonk et al., 2013; Danpaiboon et al., 2014), *Micrurus fulvirus* (Margres et al., 2013), *Ovophis okinavensis* and

* Corresponding author.
** Corresponding author. Centro Multiusuário de Inovação Biomolecular, Departamento de Física, Instituto de Biociências Letras e Ciências Exatas (Ibilce), Universidade Estadual Paulista (UNESP), Rua Cristóvão Colombo 2265, São Jose do Rio Preto, SP, 15054-000, Brazil.
E-mail addresses: monikacoronado@gmail.com (M.A. Coronado), raghuvir.arni@unesp.br (R.K. Arni).
[1] Authors contributed equally to the work.

https://doi.org/10.1016/j.toxicon.2018.08.014
Received 4 June 2018; Received in revised form 14 August 2018; Accepted 27 August 2018
Available online 01 September 2018
0041-0101/

Protobothrops flavoridis (Aird et al., 2013, 2017), *Boiga irregularis* (Pla et al., 2018), and more recently, *Lachesis muta rhobeata* (Wiezel et al., 2015), *Vipera kaznakovi*, *V. renardi*, *V. orlovi*, and *V. nikolskii* (Kovalchuk et al., 2016).

Takasaki and Tamiya (1982) described the purification, enzymatic activity, and molecular weight of a lysophospholipase as 13.6 kDa. The PLB enzyme isolated from *Pseudechis colletti,* a dimeric protein with a molecular mass of approximately 35 kDa as determined by gel filtration and 16.5 kDa as determined by SDS-PAGE, degrades phosphatidyl choline and phosphatidyl ethanolamine and was shown to possess *in vitro* haemolytic activity upon rabbit and human erythrocytes (Bernheimer et al., 1987).

The complete amino acid sequences of 11 PLBs enzymes and 2 partial sequences from snake venoms have been reported (http://www.uniprot.org/), and they share very high sequence identity (~99% identity). Since neither the three-dimensional structures nor the enzyme mechanisms and specificities have been elucidated.

We present a structural model generated by homology based on the sequence alignments of *Crotalus adamanteus* and *Micrurus fulvius* to represent all the snake venom PLB enzyme sequences currently deposited with the UniProt database. We discuss the proenzyme structure, mechanism of autocatalytic activation, catalytic mechanism and specificity, which should contribute towards improving our understanding of this unique enzyme and its role in envenomation.

Since these snake venom PLBs proteins cleave amide bonds in phospholipid head groups, they should be referred to as Phospholipase B-like (PLB-like) enzymes.

2. Methods

2.1. Sequence alignment and homology modeling

Multiple sequence alignments of snake venom phospholipase Bs proteins was performed using the MUSCLE (Edgar, 2004) and Box Shade (http://www.ch.embnet.org/software/BOX_form.htm) web servers. The atomic coordinates of bovine lysosomal phospholipase B-like enzyme from *Bos taurus* (PDB: 4BWC; sequence identity 63%) was used as the template for comparative modeling by the satisfaction of spatial restraints as implemented in the program Modeller 9v18 (Webb and Sali, 2014) to generate the model of SVPLB enzyme from *Crotalus adamanteus* (Entry: A0A0F7Z632) and *Micrurus fulvius* (Entry: U3FA79). Side chain environment acceptability, was accessed from the Verify 3D server (Lüthy et al., 1992). Geometric parameters Ramachandran plots, steric overlaps, rotamers, bonds and angle deviations were evaluated using the PROCHECK server (Laskowski et al., 1993).

The phylogenetic tree was created using maximum likelihood from web server (http://www.phylogeny.fr/index.cgi).

2.2. Molecular dynamics simulations

Since we desired to obtain information of the autocatalytic activation, we simulated the protein in two different conditions: (i) the proenzyme form of the SVPLB-like enzyme of *C. adamanteus* that includes 517 amino acids residues, and (ii) the active enzyme, after auto proteolysis, i.e., the heterodimer consisting of 492 amino acid residues. To improve sampling of the systems we performed multiple simulations for both models. We performed three molecular dynamics (100 ns each) simulations for the proenzyme with the same coordinates, but with different initial velocities (runs I, II, and III). Subsequently, after clustering combined analysis of the lowest Davies-Bouldin index (DBI) value and the highest pattern sequence based forecasting (pSF) over the three trajectory (runs I, II, and III), one representative structure was chosen, and the pro-segment (residues 208–232) was deleted and three new simulations of 100 ns each were performed (runs I',II', and III').

All the MD simulations were carried out using the AMBER16 software package (Case et al., 2017). The FF14SB force field (Maier et al., 2015) was used to describe the all-atom protein interaction. The protonation states of the amino acids side chain were set using web-server H++ (Anandakrishnan et al., 2012) at pH 7.0. The systems were neutralized with Cl^- ions and placed in a rectangular box of TIP3P water extended to at least 10 Å from any protein atom. To remove bad contacts from initial structures, the systems were energy minimized with 2500 steps of steepest descent followed by 2500 conjugate gradient steps applying a constant force constrain of 10 kcal/mol.Å^2. Then, another round with 10000 steps of energy minimization using the same procedure as before, but without force constrains was conducted. After that stage, the systems were gradually heated from 0 to 300 K for 300 ps in the constant atom number, volume, and temperature (NVT) ensemble, while the protein was restrained with constant force of 10 kcal/mol.Å^2. Subsequently, the equilibration step was performed using the constant atom number, pressure and temperature (NPT) ensemble for 500 ps and the simulation was performed for 100 ns with 2 fs time step. The constant temperature (300 K) and pressure (1 atm) were controlled by Langevin coupling. Particle-Mesh Ewald method (PME) (Darden et al., 1993) was utilized to compute the long-range electrostatic interactions and the cut-off distance of 10 Å was attributed to Van der Waals interactions.

2.3. Model analysis

The results were analyzed by using the CPPTRAJ program (Roe and Cheatham, 2013) from the AmberTools16 package (Case et al., 2017). VMD software (Humphrey et al., 1996) and Chimera (Pettersen et al., 2004), were used for visualization of the systems. Root mean square deviations (RMSD) and radius of gyration (Rg) of Cα positions were calculated to determine equilibration states and convergence of the simulations.

Clustering analysis for the representative structures of both models was performed by utilizing k-means method. To access the quality of clustering analysis we used the DBI values and pseudo-F statistic (pSF), whereas to assess the number of the clusters we conducted the silhouette analysis. Protein flexibility was studied by root mean square fluctuation (RMSF) for the Cα atoms. The RMSF were calculated residue-by-residue over the equilibrated trajectories. To assess the secondary structure of the protein over the simulation time, the DSSP method was employed (Kabsch and Sander, 1983).

3. Results and discussion

3.1. Sequence analysis

The multiple sequence alignment of 11 SVPLB-like enzymes obtained from UniProt shows very low differences in amino residue compositions as presented in Supplementary Material Fig. S1. The pro-segment, and the surface loop close to the C-terminus, are the regions with the most significant differences. Although the primary sequences, SVPLBs enzymes are very highly conserved and phylogenetic analysis (Fig. 1a) indicates that they can be divided into two general classes; Class I representing the *Elapidae*, *Dipsadidae,* and the *Culobridae* and the Class II include the *Viperidae* family.

The sequence of *M. fulvius* (*Mf*_PLB-like) was modeled to represent the class I (Fig. 1ab), the protein with N-terminal signal peptide comprise 549 amino acids residues (Fig. S1). Aleatory, we have select the PLB sequence of *Crotalus adamanteus* (*Ca*_PLB-like) class II, which consist of 553 amino acids including the N-terminal signal peptide (Fig. S1) as the target model to represent the 3D structure of the phospholipase B enzyme (Fig. 1ac).

A BLAST search performed against the atomic coordinates held with the Protein data bank (PDB) (http://www.uniprot.org/) indicated the highest sequence identity (63%) with the N-terminal nucleophile hydrolase, a lysosomal phospholipase B-*like* D1 protein from *Bos taurus* (PDB code: 4BWC) and the structural regions that are highly conserved

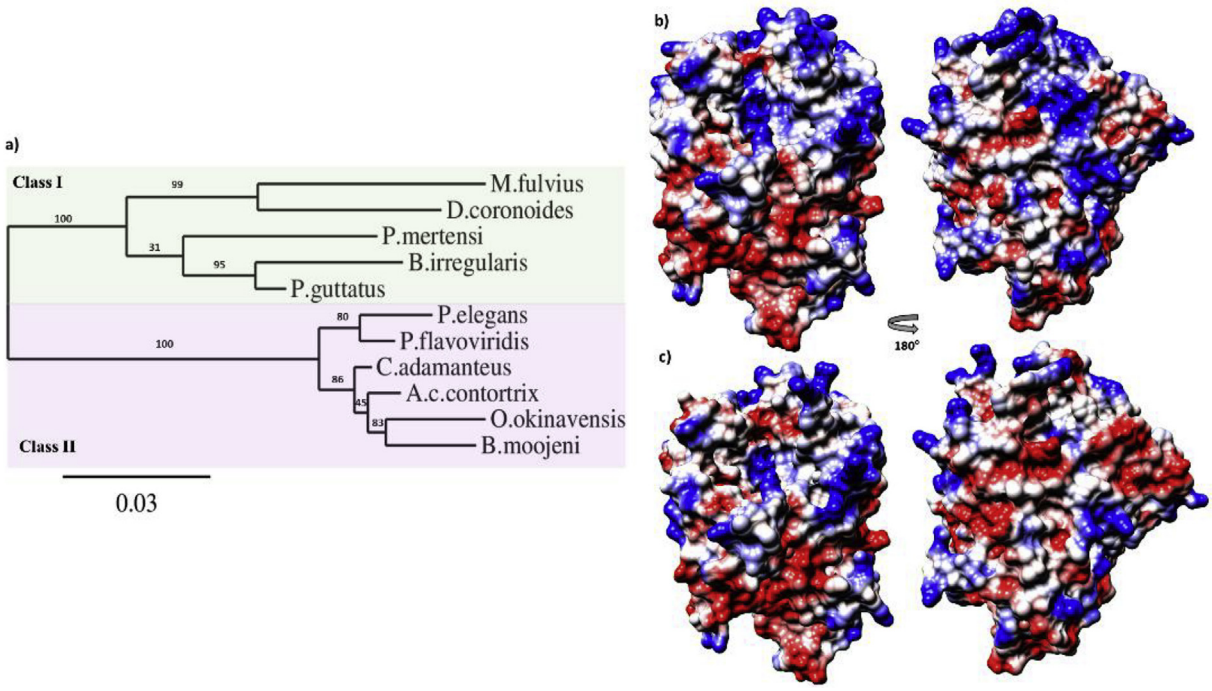

Fig. 1. Phylogenetic and Coulombic surface analysis. a) Phylogenetic analysis of phospholipase B enzyme of snake venoms. The data used includes full amino acid sequences so far available for PLB snake venom proteins. The phylogram was constructed using the online server Phylogeny.fr. **b, c)** Surface representation with 180° rotation of *M. fulvius* model that belong to class I and *C. adamanteus* to class II, respectively. Positive, negative, and neutral electrostatic potentials are drawn in *blue, red*, and *white*, respectively. (For interpretation of the references to colour in this figure legend, the reader is referred to the Web version of this article.)

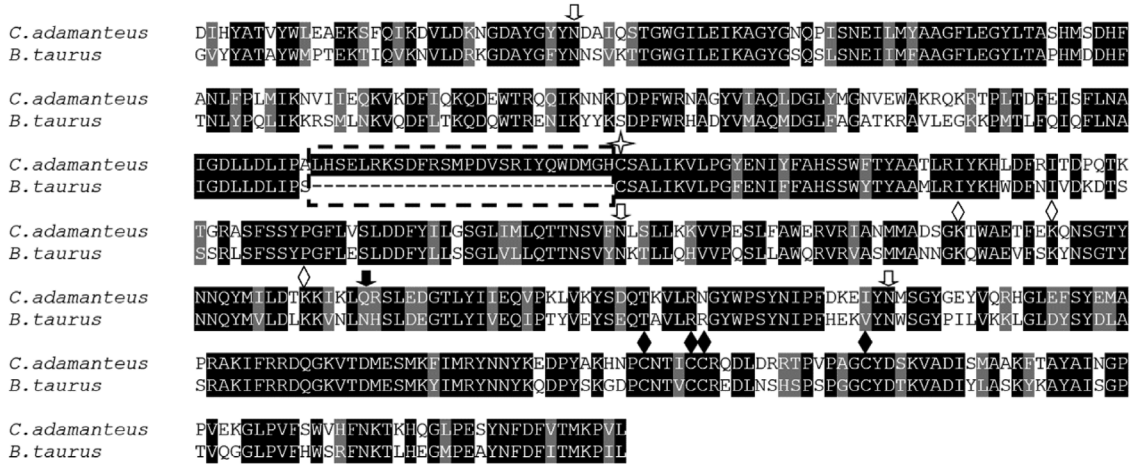

Fig. 2. Sequence alignment between phospholipase B enzyme of *C. adamanteus* snake venom and the lysosomal Ntn-hydrolase PLB-like enzyme of *Bos taurus*. Open arrows emphasize the glycosylated residues conserved in both PLB-like enzymes, the non conserved residue is highlighted in closed arrow, and the cysteines which forms the disulfide bridge are emphasized with a diamond, and the star highlights the catalytic amino acid residue.

are indicated (Fig. 2). A total of 326 amino acids residues are conserved in *C. adamanteus*, 104 residues in chain A (N-terminal domain - ~ 61%) and 222 residues in chain B (~58%). Among the conserved residues, the amino acids involved in forming the catalytic site are strictly conserved. As expected, the 25 amino acids of the peptide loop of *C. adamanteus* that suffers cleavage are not present in the sequence of the mature form of the lysosomal protein. By analogy, the glycosylation sites are conserved (residues Asn33, Asn277, and Asn380) in the PLB-like enzyme sequence of *C. adamanteus* as shown in Fig. 2.

3.2. Model building and structural validation

Modeller v9.18 software (Webb and Sali, 2014) was used for homology modeling of the 3D structure of *C. adamanteus* SVPLB-like enzyme without the N-terminal signal peptide.

The evaluation of the stereochemical properties of the predicted structure was performed using PROCHECK (Laskowski et al., 1993). Fig. 3a and b presents the *Ca*_PLB-like enzyme model and the corresponding Ramachandran Plot demonstrates that the conformation of 90% of the residues are located in the favored regions, 9.3% are in the allowed region, whereas only 0.6% are flagged as outliers. The stereochemical parameters for the omega angle is −2.0 Å, bad contact are −0.4 Å and the overall G-factor 0.8 Å. The final model presented in Fig. 3a consists of 517 residues and the pro-peptide (P-loop) with 25 amino acids residues is highlighted in red. The structural overlay of the *Ca*_PLB-like enzyme homology model with the *B. taurus* structure (RMSD 1.17 Å) is presented in Fig. 3c.

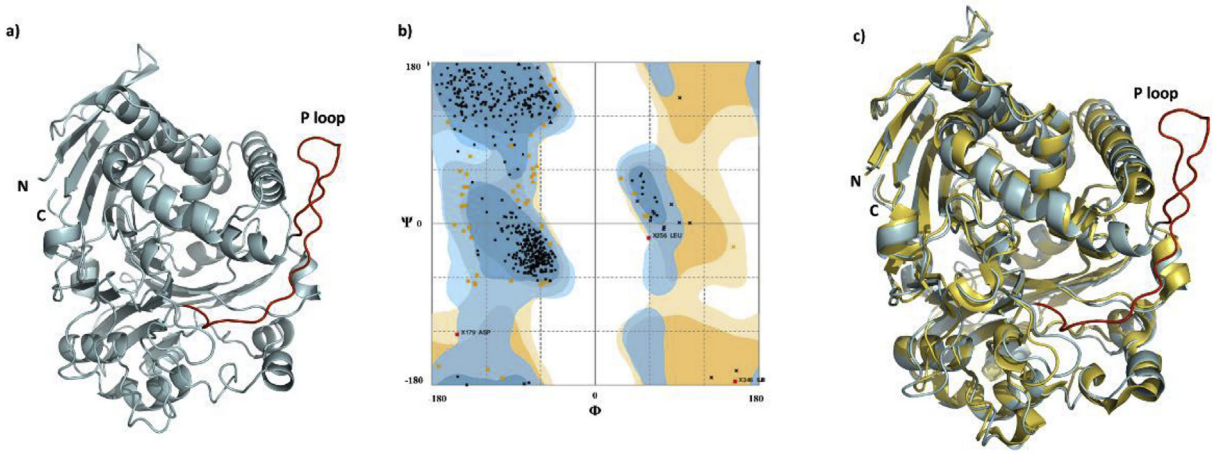

Fig. 3. Modeled structure, validation and superposition of *Ca*_PLB-like enzyme. a) Cartoon schematic representation of the modeled *Ca*_PLB-like structure, the pro-segment loop is highlighted in red. b) Ramachandran Plot for the initial homology model. c) Structural overlays of the target (PLB-like enzyme of *C. adamanteus* – light blue) and the template bPLBD1 (PDB code: 4BWC - yellow), both presented as cartoons; activation peptide in red. (For interpretation of the references to colour in this figure legend, the reader is referred to the Web version of this article.)

3.3. Molecular dynamics simulation

To investigate the structural and dynamical changes in the *Ca*_PLB-like enzyme before and after autoproteolytic activation, we performed MD simulations with two different structures of the protein. The first one, containing 517 amino acids, representing the protein before cleavage and the second one, with 492 amino acids, shows the conformation of the protein after the suggested autoproteolytic activation (mature state), after deletion of the P-loop.

The three 100 ns simulations for the pro- (labelled I, II, and III) and mature (labelled I′, II', and III') enzymes were conducted varying the initial velocities.

The equilibration of the simulations was monitored by calculating the root mean square deviations (RMSD) for the backbone atoms with respect to the starting conformation over-time to verify if all simulations kept the conformations stable during all 100 ns simulation time, presented as Supplementary material (Fig. S2). As the RMSDs indicate, the systems representing the precursor reached stability after ~40 ns without reaching the same final state, possibly due to the fluctuations related to the P-loop (Supplementary Material Fig. S2a). On the other hand, after cleavage of the P-loop between residues His208 and His232, the MD simulations were performed (3 × 100ns) and after ~ 50 ns the system reached equilibration and all three simulations reached the same final state (Supplementary Material Fig. S2b). All the analysis was performed considering only the protein in the equilibrium regime.

3.4. Precursor SVPLB-like protein model

The representative conformation of the *Ca*_PLB-like protein model before cleavage and after MD simulation presents a low RMSD value (1.015 Å). The core region displays a low RMSF value whereas regions containing loops indicated greater flexibility. Amino acid residues (His208 to His232) form the pro-segment loop that blocks the entrance to the active site (Fig. 4a), this region shows higher flexibility as observed in the RMSF plot (Supplementary Material Fig. S3a). During the production runs, the P-loop tends to dominate the motion of the protein as presented by the first component of the PCA analysis (Supplementary Material Fig. S3b). It also affects the dynamics of the residues near the active site, rendering this region more flexible. The P-loop completely blocks the catalytic region of the *Ca*_PLB-like enzyme and restricts accessibility to the susceptible scissile peptide bond between residues His232 and Cys233 (Fig. 4a). This suggests that the SVPLB-like enzyme is activated by an intramolecular autocatalytic event as described for others Ntn-hydrolases and for the mouse (Lakomek et al., 2009) and bovine (Repo et al., 2014) lysosomal proteins, as well as, for isopenicillin N-converting Ntn-hydrolase from *Penicillium chrysogenum* (Bokhove et al., 2010).

3.5. Mature structure of SVPLB-like protein

Subsequently, after clustering analysis over the three trajectory (runs I, II, and III), one representative structure was chosen (section 2.2), and the P-loop (residues His208 – His232) was deleted based on target-template alignment (Fig. 1), three new simulations of 100 ns each were performed.

The final model contains 171 residues of the N-terminal 19.6 kDa fragment and 320 amino acids residues of the C-terminal 37.1 kDa fragment (Asp37-Leu207 belong to the subunit A, Cys233-Leu553 form the continuous subunit B). In the subunit B, the amino acid residue Cys233 is the catalytic residue that plays a major role in the activity of the protein (Fig. 4b). We measured how well the three independent MD simulations converge with respect to each other, by performing three MD simulations for the mature SVPLB-like enzyme starting from the same position, but with different initial velocities. The purpose of the new MD simulation is to obtain a relaxed conformation compared with the *Ca*_PLB protein with the P-loop. Due to the absence of the loop, the MD simulations converged to the same final value as evaluated by the RMSD (Fig. S2b). The secondary structure occupancy showed low fluctuations between all the three MD simulations (Fig. 5). The average occupancy was around 44.4 ± 0.4% of alpha helices and 27.8 ± 0.4% of beta-structures as shown in Fig. 5. These values are in good agreement with the 42.5% alpha helices and 22% beta-strand secondary structure elements observed in the 4BWC X-ray model. The differences are expected due the diversity in the sequence of both proteins. Considering the fluctuation of the residues by RMSF calculations, the protein has low fluctuation with peaks up to 3 Å in regions of random coils (Fig. 5). It is also interesting to note that the exposed catalytic residue Cys233 of the theoretical model and the crystal structure are in the same relative positions following 100 ns MD simulations.

3.6. Overall SVPLB-like protein model

Ntn-hydrolases undergo structural rearrangement following autoproteolysis, where the substrate site is widened by the release of the P-loop thereby exposing the newly generated amino terminus and the catalytic Cys233. SVPLB-like enzyme possesses a fold typical for the N-

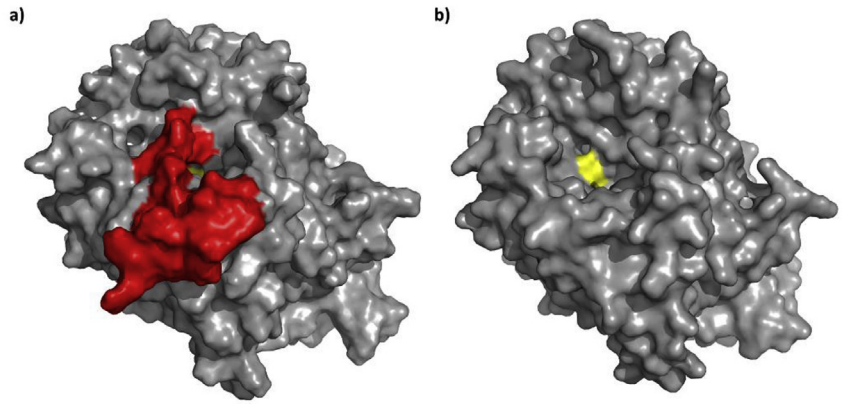

Fig. 4. Surface analysis: a) Surface representation of the SVPLB-like enzyme showing the blocked active site by the P-loop (in red). **b)** Surface representation of exposed the active site, in yellow the nucleophile amino acid cysteine. (For interpretation of the references to colour in this figure legend, the reader is referred to the Web version of this article.)

terminal nucleophile amino hydrolase (Ntn-hydrolase) superfamily and the monomer structure is similar to that of the bovine PLB (4DWC) used as templates to build the model. We suggested that the 25 amino acids residues of the N-terminal segment are proteolytically removed from the mature protein as like bovine PLB. The protein Ntn-hydrolase model consists of a four-layer αββα sandwich core (Fig. 3a) in which two intramolecular disulfide bridges are formed between Cys479 – Cys494 and between Cys475 – Cys480 of chain B. The active site of Ntn-hydrolases is located between the core β-sheets. The Ntn residue, which in the SVPLB-like protein families is a cysteine, possibly performs two catalytic roles: as a nucleophile and as a general base (http://www.enzyme.chem.msu.ru/hcs/cgi/class.cgi?clsid=C.02).

The thiol group of the catalytic amino acid residue, Cys233, is located at the beginning of the second chain (C-terminal segment). His250 and the hydrogen bond formed to Lys498, which is supported by Asp496, Asp293, and Arg261, sustain the catalytic machinery (Fig. 6a). The amino acids around the catalytic Cys233 are highly conserved.

Typically, the oxyanion hole for an Ntn-hydrolase is formed by residues Thr300 and Asn399 in bPLBD1, which superimposes on SVPLB-like enzyme with Thr308 and Asn407 residues. The backbone of Trp253 stabilizes the thiol state and the positively charged α-amino group of the N-terminal cysteine as in bPLBD1 (Fig. 6a).

The removal of the 25 amino acid residues preceding Cys233 widens the substrate-binding site as shown in Fig. 4b. There are relevant differences in the pockets, between the template and the model. Surface charge analysis demonstrated that *Ca*_PLB-like enzyme exhibits highly negatively charged surface around the cavity forming the active site (Fig. 7a), whereas in bPLB-like protein the corresponding area is positively charged (Fig. 7b). Additionally, the differences in the side chain of the amino acids residues surrounding the pocket modify the topography, which probably determines the selectivity of the substrate.

4. Conclusion

Snake venom Phospholipase Bs (SVPLBs) proteins are present in very low amounts in a number of snake venoms and, to date, have not been studied extensively. Differences in the amino acid sequences are largely limited to amino acids residues located on the surfaces of the three-dimensional structures of *M. fulvius* (Fig. 1b) and *C. adamanteus* (Fig. 1c) PLBs generated by homology modeling as example to represent both classes, and thus significantly alter the surface electrostatic charges.

When compared with the sequence and structure of the bovine phospholipase B-like protein, the position of Asn408 residue in *Ca*_PLBs-like enzyme is conserved indicating that the SVPLBs-like enzymes also undergo N-glycosylation and are hence localized to the lysosome. The counterparts of Lys334, Lys 342, and Lys358 in the bovine enzyme, two of which are implicated in the initiation of mannose-6-phosphorylation are also conserved in *Ca*_PLB-like enzymes (Fig. 2).

Thus, based on the conformation of the active site residues, the catalytic mechanism and lysosomal targeting suggested above, it is

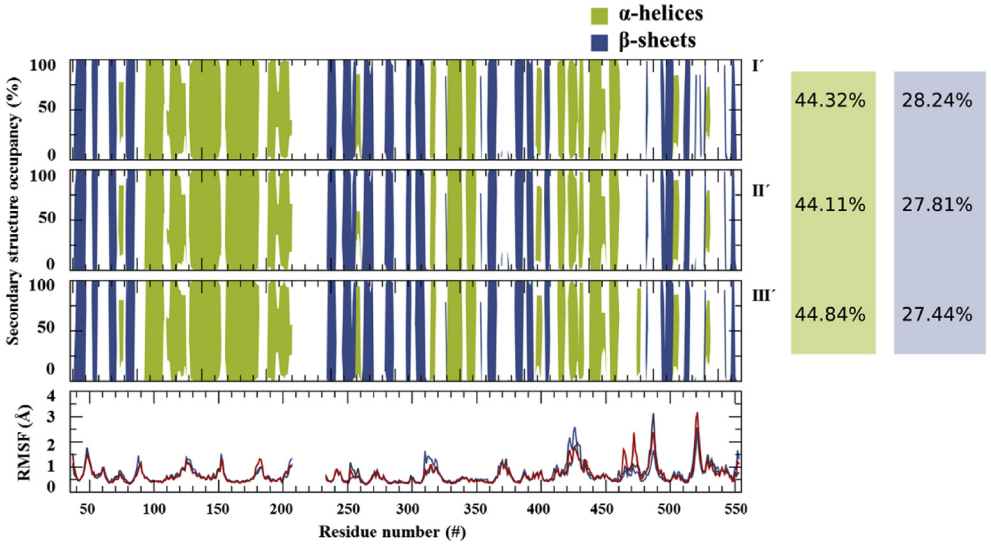

Fig. 5. Residues of secondary structure occupancy and root mean square fluctuations (RMSF) of the mature *Ca*_PLB-like enzyme. The overall percentages of the secondary structure of the mature form of the enzyme are indicated to the right.

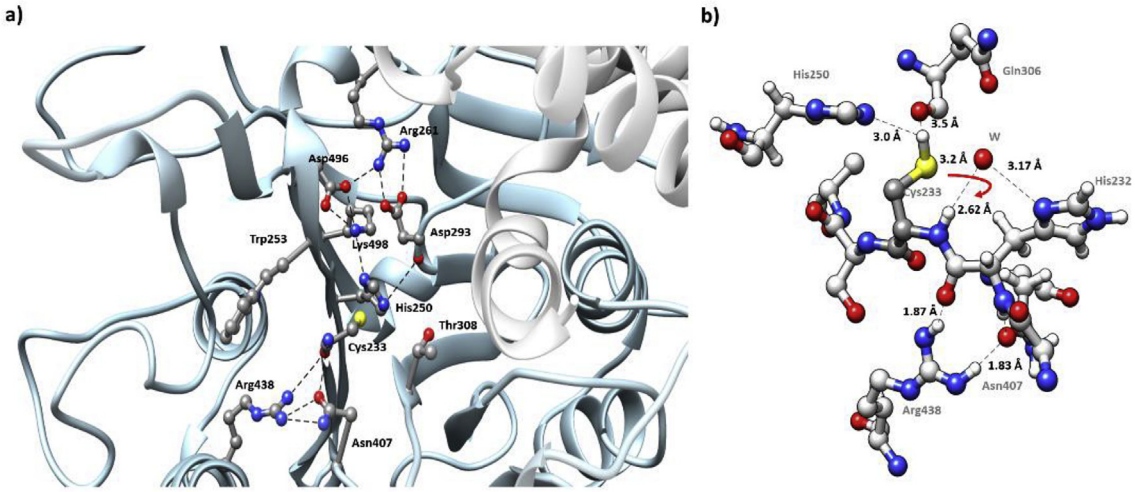

Fig. 6. Stabilization of the N-terminal cysteine. a) The side chain of the residues participating on Cys233 stabilization are shown in ball stick and the hydrogen bonds in dotted line. **b)** Suggestion of the primary cysteine autoproteolytic cleavage.

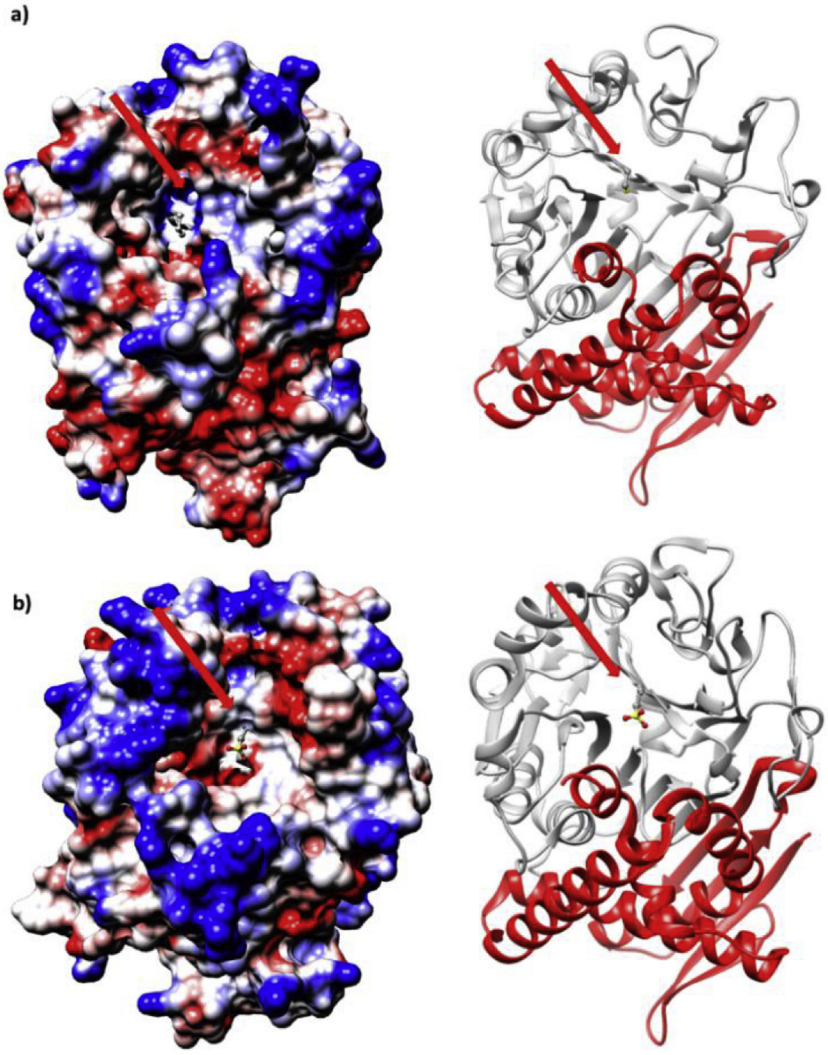

Fig. 7. Comparison of the electrostatic potential surface between a) SVPLB-like protein model and **b)** bPLB protein. Electrostatic potential surfaces of the proteins pointing the inner pore are shown in the left side, whereas cartoon view pointing the catalytic amino acid residue is shown in the right side.

likely that these enzymes are probably not lipases but are in actuality amidases or peptidases and the exact role of these enzymes in envenomation should be investigated.

Based on our model, we therefore propose two mechanisms by which the SVPLB-*like* mediated autoproteolysis occurs: either i) initially, a cysteine initiates proteolysis, subsequent conformational constraints trigger a peptide flip generating a high-energy state of the prosegment. A water molecule, positioned by hydrogen bonds in a tetrahedral geometry, acts as a general base where the Cys233 hydroxyl group is deprotonated increasing its nucleophilicity. The hydroxyl group carries out the nucleophilic attack on the peptide bond between His232 and Cys233 (Fig. 6b red arrow) and His 232 is responsible in maintaining the tetrahedral geometry, or, ii) a bound water molecule (Fig. 6b) could act as the nucleophile in the one-step cleavage mechanism. The water molecule is in a favourable position to attack the carbonyl carbon of the scissile bond, resulting in the release of the N-terminal of the P-loop. The NE atom of His250, which are 3.0 Å away from the Cys233, can stabilize the resultant thiolate ion.

Primary mechanism was already proposed for others N-terminal hydrolase enzymes (Kim et al., 2006; Lakomek et al., 2009; Repo et al., 2014; Bokhove et al., 2010). However, the secondary cleavage mechanism of Ntn-hydrolase is not clearly understood. Nevertheless, Kim and collaborators suggested a carboxyl proteolytic cleavage for the second auto-cleavage, together with a water molecule (Kim et al., 2006).

In conclusion, these enzymes are not phospholipase B-like but are Ntn hydrolases since they do not hydrolyze the same phospholipid bond as phospholipases A1 and A2 (ie; sn*1* and sn*2*) but instead, hydrolyze the amide bond to liberate the polar head group.

Detailed information on the mechanisms of catalysis and specificity of this snake venom enzyme will contribute to improving our understanding of the process of envenomation.

Author contributions

M.A.C. Conceived and designed the experiments; M.A.C., D.S.O., R.J.E. and M.S.A. performed the experiments and analyzed the data; M.A.C and R.K.A. guided the research and the preparation of the manuscript.

Conflicts of interests

The authors declare no conflicts.

Acknowledgments

This work is supported by grants from CNPq [Grant numbers 435913/2016-6, 401270/2014-9, 307338/2014-2], FAPESP [Grant numbers 2015/13765-0, 2015/18868-2, 2016/08104-8; 2016/12904-0; 2009/53989-4], FUNDECT [23/200.307/2014], CAPES and PROPe UNESP.

Appendix A. Supplementary data

Supplementary data related to this article can be found at https://doi.org/10.1016/j.toxicon.2018.08.014.

Transparency document

Transparency document related to this article can be found online at https://doi.org/10.1016/j.toxicon.2018.08.014.

References

Ackermann, E.J., Dennis, E.A., 1995. Mammalian calcium-independent phospholipase A2. Biochim. Biophys. Acta 1259, 125–136.

Aird, S.D., Watanabel, Y., Villar-Briones, A., Roy, M.C., Terada, K.T., Mikheyev, A.S., 2013. Quantitative high-throughput profiling of snake venom gland transcriptomes and proteomes (*Ovophis okinavensis* and *Protobothrops flavoviridis*). BMC Genom. 14, 790.

Aird, S.D., Arora1, J., Barua, A., Qiu, L., Terada, K., Mikheyev, A.S., 2017. Population genomic analysis of a pitviper reveals microevolutionary forces underlying venom chemistry. Genome Biol. Evol. 10, 2640–2649.

Akiba, S., Sato, T., 2004. Cellular function of calcium-independent phospholipase A2. Biol. Pharm. Bull. 27 (8), 1174–1178.

Anandakrishnan, R., Aguilar, B., Onufriev, A.V., 2012. H++ 3.0: automating pK prediction and the preparation of biomolecular structures for atomistic molecular modeling and simulation. Nucleic Acids Res. 40 (W1), W537–W541.

Bernheimer, A.W., Linder, R., Weinstein, S.A., Kim, K.S., 1987. Isolation and characterization of a phospholipase B from venom of Collett's snake, *Pseudechis colletti*. Toxicon 25, 547–554.

Bokhove, M., Yoshida, H., Hensgens, C.M., van der Laan, J.M., Sutherland, J.D., Dijkstra, B.W., 2010. Structures of an isopenicillin N converting Ntn-hydrolase reveal different catalytic roles for the active site residues of precursor and mature enzyme. Structure 18, 301–308.

Boll, W., Schmid-Chanda, T., Semenza, G., Mantei, N., 1993. Messenger RNAs expressed in intestine of adult but not baby rabbits. J. Biol. Chem. 268, 12901–12911.

Brannigan, J.A., Dodson, G., Duggleby, H.J., Moody, P.C., Smith, J.L., Tomchick, D.R., Murzin, A.G., 1995. A protein catalytic framework with an N-terminal nucleophile is capable of self-activation. Nature 378, 416–419.

Case, D.A., Cerutti, D.S., Cheatham III., T.E., Darden, T.A., Duke, R.E., Giese, T.J., Gohlke, H., Goetz, A.W., Greene, D., Homeyer, N., Izadi, S., Kovalenko, A., Lee, T.S., LeGrand, S., Li, P., Lin, C., Liu, J., Luchko, T., Luo, R., Mermelstein, D., Merz, K.M., Monard, G., Nguyen, H., Omelyan, I., Onufriev, A., Pan, F., Qi, R., Roe, D.R., Roitberg, Sagui, C., Simmerling, C.L., Botello-Smith, W.M., Swails, J., Walker, R.C., Wang, J., Wolf, R.M., Wu, X., Xiao, L., York, D.M., Kollman, P.A., 2017. AMBER. University of California, San Francisco.

Chatrath, S.T., Chapeaurouge, A., Lin, Q., Lim, T.K., Dunstan, N., Mirtschin, P., Kumar, P.P., Kini, R.M., 2011. Identification of novel proteins from the venom of a cryptic Snake *Drysdalia coronoides* by a combined transcriptomics and proteomics approach. J. Proteome Res. 2, 739–750.

Coronado, M.A., Moraes, F.R., Ullah, A., Masood, R., Santana, V.S., Mariutti, R., Brognaro, H., Georgieva, D., Murakami, M.T., Betzel, C., Arni, R.K., 2014. Three-dimensional structures and mechanisms of snake venom serine proteinases, metalloproteinases, and phospholipase A_2s. In: Gopalakrishnakone, P., Calvete, J. (Eds.), Venom Genomics and Proteomics. Springer, Dordrecht.

Coronado, M.A., Eberle, R.J., Moraes, F.R., Fernandez, J.H., Gomes, E.P., Lira, A., Arni, R.K., 2016. Evolution, structural features, and biochemical diversity of snake venom serine proteinases. In: Utkin, Y.N., Krivoshein, A.V. (Eds.), Snake Venoms and Envenomation. Nova Science Publisher, Inc.

Danpaiboon, W., Reamtong, O., Sookrung, N., Seesuay, W., Sakolvaree, Y., Thanongsaksrikul, J., Dong-din-on, F., Srimanote, P., Thueng-in, K., Chaicumpa, W., 2014. Ophiophagus hannah venom: proteome, components bound by Naja kaouthia antivenin and neutralization by N. kaouthia neurotoxin-specific human ScFv. Toxins (Basel) 5, 1526–1558.

Darden, T., York, D., Pedersen, L., 1993. Particle mesh Ewald: an N· log (N) method for Ewald sums in large systems. J. Chem. Phys. 98, 10089–10092.

Dawson, R.M.C., 1958. Studies on the hydrolysis of lecithin by a Penicillium notatum phospholipase B preparation. Biochem. J. 4, 559–570.

Doery, H.M., Pearson, J.E., 1964. Phospholipase B in snake venoms and bee venom. Biochem. J. 3, 599–602.

Duggleby, H.J., Tolley, S.P., Hill, C.P., Dodson, E.J., Dodson, G., Moody, P.C.E., 1995. Penicillin acylase has a single-amino-acid catalytic centre. Nature 373, 264–268.

Edgar, R.C., 2004. MUSCLE: multiple sequence alignment with high accuracy and high throughput. Nucleic Acids Res. 5, 1792–1797.

Gallard, T., 1971. Enzymatic deacylation of lipids in plants: the effects of free fatty acids on the hydrolysis of phospholipids by the lipolytic acyl hydrolase of potato tubers. Eur. J. Biochem. 21, 90–98.

Georgieva, D., Ohler, M., Seifert, J., von Bergen, M., Arni, R.K., Genov, N., Betze, l C., 2010. The venomics of Bothrops alternatus is a pool of acidic proteins with predominant hemorrhagic and coagulopathic activities. J. Proteome Res. 9 (5), 2422–2437 7.

Ghannoum, M.A., 2000. Potential role of phospholipases in virulence and fungal pathogenesis. Clin. Microbiol. Rev. 1, 122–143.

Humphrey, W., Dalke, A., Schulten, K., 1996. VMD: visual molecular dynamics. J. Mol. Graph. 14, 33–38.

Kabsch, W., Sander, C., 1983. Dictionary of protein secondary structure: pattern recognition of hydrogen-bonded and geometrical features. Biopolymers 22, 2577–2637.

Kang, T.S., Georgieva, D., Genov, N., Murakami, M.T., Sinha, M., Kumar, R.P., Kaur, P., Kumar, S., Dey, S., Sharma, S., Vrielink, A., Betzel, C., Takeda, S., Arni, R.K., Singh, T.P., Kini, R.M., 2011. Enzymatic toxins from snake venom: structural characterization and mechanism of catalysis. FEBS J. 278 (23), 4544–4576.

Kim, Y., Yoon, Ki-H., Khang, Y., Turley, S., Hol, W.G.J., 2000. The 2.0 Å crystal structure of cephalosporin acylase. Structure 8, 1059–1068.

Kim, J.K., Yang, I.S., Shin, H.J., Cho, K.J., Ryu, E.K., Kim, S.H., Park, S.S., Kim, K.H., 2006. Insight into autoproteolytic activation from the structure of cephalosporin acylase: a protein with two proteolytic chemistries. PNAS 6, 1732–1737.

Kovalchuk, S.I., Ziganshin, R.H., Starkov, V.G., Tsetlin, V.I., Utkin, Y.N., 2016. Quantitative proteomic analysis of venoms from Russian vipers of pelias group: phospholipases A_2 are the main venom components. Toxins (Basel) 4, 105.

Lakomek, K., Dickmanns, A., Kettwig, M., Urlaub, H., Ficner, R., Lübke, T., 2009. Initial

insight into the function of the lysosomal 66.3 kDa protein from mouse by means of X-ray crystallography. BMC Struct. Biol. 25 9:56.
Laskowski, R.A., MacArthur, M.W., Moss, D.S., Thornton, J.M., 1993. PROCHECK - a program to check the stereochemical quality of protein structures. J. App.Cryst. 26 283e291.
Lüthy, R., Bowie, J.U., Eisenberg, D., 1992. Assessment of protein models with three-dimensional profiles. Nature 356 83e85.
Maier, J.A., Martinez, C., Kasavajhala, K., Wickstrom, L., Hauser, K.E., Simmerling, C., 2015. ff14SB: improving the accuracy of protein side chain and backbone parameters from ff99SB. J. Chem. Theor. Comput. 8, 3696–3713.
Margres, M.J., Aronow, K., Loyacano, J., Rokyta, D.R., 2013. The venom-gland transcriptome of the eastern coral snake (*Micrurus fulvius*) reveals high venom complexity in the intragenomic evolution of venoms. BMC Genom. 14, 531.
Matsuda, H., Hirayama, O., 1979. Purification and properties of a lipolytic acyl-hydrolase from potato leaves. Biochim. Biophys. Acta 27, 155–165.
Matsumoto, Y., Mineta, S., Murayama, K., Sugimori, D., 2013. A novel phospholipase B from Streptomyces sp. NA684 – purification, characterization, gene cloning, extracellular production and prediction of the catalytic residues. FEBS J. 280, 3780–3796.
Nauze, M., Gonin, L., Chaminade, B., Perès, C., Hullin-Matsuda, F., Perret, B., Chap, H., Gassama-Diagne, A., 2002. Guinea pig phospholipase B: identification of the catalytic serine, the proregion involved in its processing and enzymatic activity. J. Biol. Chem. 46, 44093–44099.
Ohler, M., Georgieva, D., Seifert, J., von Bergen, M., Arni, R.K., Genov, N., Betzel, C., 2010. The venomics of Bothrops alternatus is a pool of acidic proteins with predominant hemorrhagic and coagulopathic activities. J. Proteome Res. 9 (5), 2422–2437 7.
Oliveira, I.S., Cardoso, I.A., Bordon, K.C.F., Carone, S.E.I., Boldrini-França, J., Pucca, M.B., Zoccal, K.F., Faccioli, L.H., Sampaio, S.V., Rosa, J.C., Arantes, E.C., 2018. Global proteomic and functional analysis of *Crotalus durissus collilineatus* individual venom variation and its impact on envenoming. J Proteomics S1874–3919 (18) 30066-6.
Pla, D., Petrasb, D., Saviolaa, A.J., Modahl, C.M., Sanza, L., Péreza, A., Juáreza, E., Frietzec, S., Dorresteinb, P.C., Mackessyc, S.P., Calvete, J.J., 2018. Transcriptomics-guided bottom-up and top-down venomics of neonate and adult specimens of the arboreal rear-fanged Brown Treesnake, *Boiga irregularis*, from Guam. J. Proteomics 174, 71–84.
Pettersen, E.F., Goddard, T.D., Huang, C.C., Couch, G.S., Greenblatt, D.M., Meng, E.C., Ferrin, T.E., 2004. UCSF Chimera–a visualization system for exploratory research and analysis. J. Comput. Chem. 13, 1605–1612.
Rawlings, N.D., Barrett, A.J., Thomas, P.D., Huang, X., Bateman, A., Finn, R.D., 2018. The MEROPS database of proteolytic enzymes, their substrates and inhibitors in 2017 and a comparison with peptidases in the PANTHER database. Nucleic Acids Res. 46, D624–D632.
Repo, H., Kuokkanen, E., Oksanen, E., Goldman, A., Heikinheimo, P., 2014. Is the bovine lysosomal phospholipase B-like protein an amidase? Proteins 2, 300–311.
Roe, D.R., Cheatham III, T.E., 2013. PTRAJ and CPPTRAJ: software for processing and analysis of molecular synamics trajectory data. J. Chem.Theory Com. 9, 3084–3095.
Rokyta, D.R., Wray, K.P., Lemmon, A.R., Lemmon, E.M., Caudle, S.B., 2011. A high-throughput venom-gland transcriptome for the Eastern Diamondback Rattlesnake (*Crotalus adamanteus*) and evidence for pervasive positive selection across toxin classes. Toxicon 5, 657–671.
Suresh, C.G., Pundle, A.V., SivaRaman, H., Rao, K.N., Brannigan, J.A., McVey, C.E., Verma, C.S., Dauter, Z., Dodson, E.J., Dodson, G.G., 1999. Penicillin V acylase crystal structure reveals new Ntn-hydrolase family members. Nat. Struct. Mol. Biol. 6, 414–416.
Takasaki, C., Tamiya, N., 1982. Isolation and properties of Lysophospholipases from the venom of an Australian elapid sanke, Pseudechis australis. Biochem. J. 203, 269–276.
Vonk, F.J., Casewell, N.R., Henkel, C.V., Heimberg, A.M., Jansen, H.J., McCleary, R.J.R., Kerkkamp, H.M.E., Vos, R.A., Guerreiro, I., Calvete, J.J., Wüster, W., Woods, A.E., Logan, J.M., Harrison, R.A., Castoe, T.A., Koning, J.A.P. de, Pollock, D.D., Yandell, M., Calderon, D., Renjifa, C., Currier, R.B., Salgado, D., Pla, D., Sanz, L., Hyder, A.S., Ribeiro, J.M.C., Arntzen, J.W., van den Thillart, G.E.E.J.M., Boetzer, M., Pirovana, W., Dirks, R.P., Spaink, H.P., Duboule, D., McGlinn, E., Kini, R.M., Richardson, M.K., 2013. The king cobra genome reveals dynamic gene evolution and adaptation in the snake venom system. PNAS 51, 20651–20656.
Webb, B., Sali, A., 2014. Comparative Protein Structure Modeling Using Modeller. Current Protocols in Bioinformatics, vol. 5 John Wiley & Sons, Inc. 6.1-6.5.6.32.
Wiezel, G.A., dos Santos, P.K., Cordeiro, F.A., Bordon, K.C., Selistre-de-Araújo, H.S., Ueberheide, B., Arantes, E.C., 2015. Identification of hyaluronidase and phospholipase B in Lachesis muta rhombeata venom. Toxicon 359–368.